Capacitive and resistive double sheath model in an asymmetric radio frequency plasma discharge

E Faudot

Capacitive and resistive double sheath model in an asymmetric radio frequency plasma discharge

E. Faudot

Citation: Physics of Plasmas **22**, 083506 (2015); doi: 10.1063/1.4928417
View online: http://dx.doi.org/10.1063/1.4928417
View Table of Contents: http://scitation.aip.org/content/aip/journal/pop/22/8?ver=pdfcov
Published by the AIP Publishing

Capacitive and resistive double sheath model in an asymmetric radio frequency plasma discharge

E. Faudot
IJL, Department P2M, Universite de Lorraine, 54500 Vandoeuvre les Nancy, France

(Received 7 April 2015; accepted 23 July 2015; published online 13 August 2015)

The double asymmetric probe model presented here solves the rectified rf potential and rf currents in an asymmetric rf discharge as a function of the electrode surface ratio S_1/S_2, the rf potential compared to the floating potential, and the sheath capacitances on both sides of the discharge. It is demonstrated that this asymmetric unmagnetized model can be applied to a magnetized double probe one in which the asymmetry arises from the anisotropy between parallel and perpendicular currents. Asymptotic solutions for highly asymmetric discharges yield a dc saturation current on the rf electrode equal to $-I_{sat}/2$ for low sheath capacitance and $-I_{sat}$ for high sheath capacitance. The transition capacitance between "low" and "high" is defined as C_0. A solution of the rf averaged current and rectified potential as a function of the surface ratio and the rf potential are also proposed for each regime. These analytical solutions are confirmed by the full numerical model taking into account the generator resistance and the plasma conductivity. © *2015 AIP Publishing LLC*.
[http://dx.doi.org/10.1063/1.4928417]

I. INTRODUCTION

Asymmetric discharges are driven in most experimental rf plasma devices. They are partially treated in the frame of capacitive coupled plasmas (CCP)[1,2] for spherical electrodes[3] or even cylindrical ones.[4] The case of an asymmetric discharge with a finite blocking capacitor as been studied by Metze *et al.*[5] and Chen[6] considering self-consistent sheath capacitance. The problem of highly asymmetric discharges has been extended by incorporating the ion dynamics in the sheath using a heuristic ion model[7] or the full ion fluid model.[8,9]

The present model is quite similar to Klick's resistive model[10] except here an equivalent static sheath capacitance is included. Klick's model allows only dc currents to flow from 1 electrode to several other ones while the present model allows both rf and dc currents to flow from one electrode to another one. Considering rf displacement currents, the present model is more simple than the Metze's model in which the capacitance for the sheath is time dependent and then much harder to solve. Second, the Metze's model is composed of a dc blocking capacitor between the rf generator and the rf electrode instead of a resistor for the present model. This resistor plays the role of the internal rf generator resistance and is totally independent of the sheath and plasma resistance.

Here, the model has the advantage to take into account displacement currents in the sheath and the rf generator resistance with analytical solutions for asymptotical cases and enlightens the fact that dc current can either saturate to $I_{sat}/2$ or I_{sat} as a function of a transition capacitance defined as well in this paper.

Even if this model does not fit well for most rf discharges driven with a blocking capacitor, it can apply for the next cases.

First, it can apply to probes. In the special case of rf compensated probes which cut off the rf current component via inductors, a simple DC sheath model can be used. But for a classical dc probe in a rf environment, this rf model could help to interpret potential and current measurements without compensation. The current shift could be deduced and the I-V characteristics could be adjusted. Second, this model can apply in plasma discharges that allow dc currents, especially in hot plasma devices such as tokamak or stellarator in which RF antennas[20] are protected by a Faraday screen and limiters which are biased by induction and are electrically connected to the ground. For example, this model allows to calculate the amount of current flowing between two differential biased parts (the antenna and the wall) of a plasma reactor. Finally, this model is well adapted to our new linear plasma device "Aline"[12] in which the RF amplifier is directly connected to the RF electrode (no blocking capacitor) to simulate a low power ICRF (Ion Cyclotron Resonant Frequency) antenna as in tokamaks.

The model works for all electrode surface ratios (symmetric or asymmetric discharges) but does not take into account the shape of the electrodes (flat geometry assumption). The potential and current are calculated on both electrodes and at entrance of both sheaths as a function of time during several rf periods.

In a first part, a time dependent analytical solution is proposed for rectified potential and current taking into account each sheath capacitance, plasma conductivity, and an imposed dc bias potential on one electrode. In a second part, the asymmetric model is applied to a symmetric magnetized plasma with perpendicular polarization currents.[13,14] It has been shown in other studies that ICRF antenna in tokamaks can drive dc currents[11,15] and even deplete the bias flux tube region.[16,17] Actually, the present model is a generalization of the magnetized double probe model,[13] in which the polarization current term can be included in a general displacement current expression via an equivalent capacitance. In the magnetized plasma case, this capacitance

represents transverse displacement currents. Here, this is a 0D approach only dedicated to determine potential and current in sheath and on the electrodes, while the previous Faudot's model is a 2D space model allowing the study of rectified potential structures. In addition, the generalized model provides analytical solutions for rectified potential and currents, which are presented in the third part from a derivation of asymptotic solutions (high/low asymmetry and high/low sheath capacitance). The comparison of the numerical model solution with the asymptotic analytical formulas is discussed in the fourth part. Finally the numerical solutions are available for non-asymptotic cases and permit to deduce current and potential for our experimental device Aline in which the rf generator resistance is 50 Ω.

II. ASYMMETRIC CIRCUIT MODEL

Several assumptions are necessary to simplify typical rf plasma discharges in which density, temperature, and geometry are self-consistent so that many nonlinear couplings make the solving very tricky. Here, are the circuit model assumptions: Electron and ion velocity distributions are Maxwellian in the plasma with a constant temperature Te and Ti, respectively. The electrons have a Boltzmann density distribution in the sheath; rf frequency is higher than ion plasma frequency so that ions are too heavy to react to the varying electric field in the sheath; collisions are neglected in the sheath (valid for hot plasmas or low pressure plasma discharges); the magnetic field is taken into account through an equivalent displacement current term; the electric field solver is electrostatic (Poisson's equation). The plasma is considered as a homogeneous resistive dipole. Sheath conduction currents are modeled by the diode equation. Sheath displacement currents are modeled by a capacitance that is constant in time. The plasma contributes an ohmic, series resistance. The external circuit (including the generator) contributes another series resistance.

According to physical scheme in Figure 1 and electrical model in Figure 2, the current conservation equation on the rf side can be written as follows:

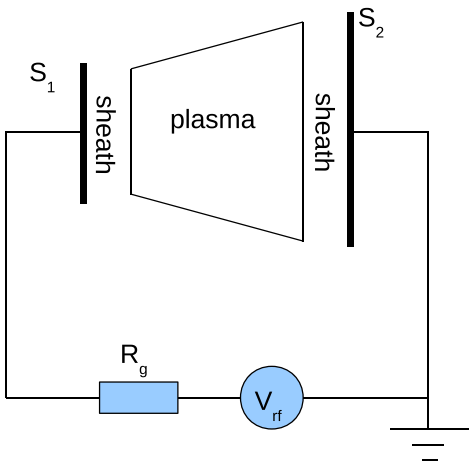

FIG. 1. Physical sketch of an asymmetric rf plasma discharge.

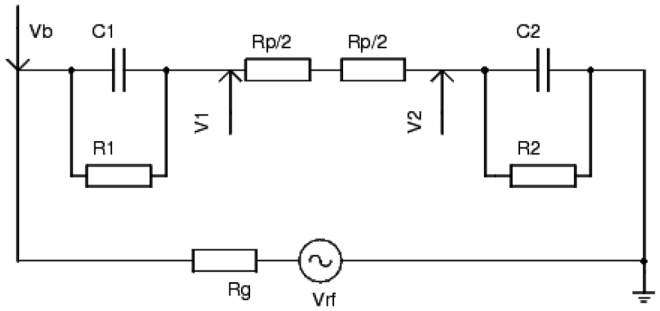

FIG. 2. Equivalent electric model of the plasma and sheaths.

$$\frac{V_2 - V_1}{R_p} = j_i S_1 \left(1 - \exp\left[\frac{e}{k_B T_e}(V_{fl} - V_1 + V_b)\right]\right) + C_1 \frac{d}{dt}(V_1 - V_b), \tag{1}$$

where R_p is the global plasma resistance, V_1 and V_2 are the potential at the entrance of the sheath on the RF side and on the grounded wall side, respectively, j_i and j_e are the absolute values of ion and electron saturation current densities, T_e is the electron temperature, V_{fl} is the floating potential defined as follows:

$$V_{fl} = \frac{k_B T_e}{e} \ln\left(\frac{j_e}{j_i}\right), \tag{2}$$

V_b is the bias potential on the antenna, C_1 is the capacitance of the sheath on the rf side, V_{rf} is the rf potential, and S_1 is the antenna area. The sheath capacitance can be evaluated from the flat capacitor model in vacuum considering that the electron density is close to 0 within the sheath.[18] A good definition for C_1 and C_2 is

$$C_1 = \frac{\epsilon_0 S_1}{\lambda_{sh1}}, \tag{3}$$

$$C_2 = \frac{\epsilon_0 S_2}{\lambda_{sh2}}. \tag{4}$$

λ_{sh1} and λ_{sh2} are, respectively, the sheath thickness in front of the rf electrode and the grounded electrode and can be defined as follows:[1]

$$\lambda_{sh1} = \left(\frac{4\sqrt{(2)}}{9}\right)^{1/2} \lambda_{De} \left(\frac{e\langle V_1 - V_{rf}\rangle}{k_B T_e}\right)^{3/4}, \tag{5}$$

$$\lambda_{sh2} = \left(\frac{4\sqrt{(2)}}{9}\right)^{1/2} \lambda_{De} \left(\frac{e\langle V_2\rangle}{k_B T_e}\right)^{3/4}. \tag{6}$$

$\langle V_1 - V_{rf}\rangle$ and $\langle V_2\rangle$ are the time average potential drop in the sheath on the rf side and grounded side. A self-consistent capacitance has been studied by Chen[6] resulting in a nonlinear capacitive sheath distorting slightly the rf potential as a function of time. Nevertheless, the time averaged value can be reasonably considered close to the static capacitive sheath studied here.

The current conservation equation on the grounded wall side leads to

$$I = \frac{V_2 - V_1}{R_p} = j_i S_2 \left(1 - \exp\left[\frac{e}{k_B T_e}(V_{fl} - V_2)\right]\right) + C_2 \frac{dV_2}{dt}. \quad (7)$$

I is the current flowing along the circuit. Here, C_2 is the sheath capacitance on the grounded wall side, and S_2 is the area of the grounded wall.

The potential on the rf electrode is written as

$$V_b = V_{rf} - R_g.I. \quad (8)$$

R_g is the resistance of the rf generator and V_{rf} its output rf voltage. One can notice that the nonlinear sheath conductivity is simply represented by resistances R_1 and R_2 in Figure 2.

Solving such a nonlinear differential equation system is not possible analytically. At least one can solve the same problem considering only one unknown: $V = V_1 = V_2$, the potential in a perfect conductor plasma. In such a particular case, the 3 equations system can be reduced to one equation with the normalized potentials $\phi = \frac{eV}{k_B T_e}$, $\phi_{rf} = \frac{eV_{rf}}{k_B T_e}$, $\phi_{fl} = \frac{eV_{fl}}{k_B T_e}$, and $\phi_b = \frac{eV_b}{k_B T_e}$.

$$j_i\left(S_1 + S_2 - \exp\left(-\phi + \phi_{fl}\right)\left[S_2 + S_1 \exp\left(\phi_{rf} + \phi_b\right)\right]\right) + \frac{k_B T_e}{e}\left[C_1 \frac{d\left(\phi - \phi_{rf}\right)}{dt} + C_2 \frac{d\phi}{dt}\right] = 0. \quad (9)$$

Here, ϕ_b does not depend on time and is considered as a constant.

The solution of this equation can be written with the help of the Modified Bessel function of the 1st kind I_n considering a cosine rf potential $\phi_{rf}(t) = \overline{\phi_{rf}}.\cos(\omega t)$, with ω as the rf pulsation

$$\exp(\phi) = S + T + W. \quad (10)$$

As it can be seen in Eq. (10), the solution is composed of 3 terms: S is the stationary term, T is the transient term, and W is the oscillatory term.

Considering the following constant expressions:

$$\alpha = \frac{e j_i (S_1 + S_2)}{k_B T_e (C_1 + C_2)}, \quad (11)$$

$$\gamma_1 = \frac{C_1}{C_1 + C_2}, \quad (12)$$

$$\gamma_2 = \frac{C_2}{C_1 + C_2}. \quad (13)$$

The analytical solution for ϕ is

$$\exp(\phi) = \frac{A}{\alpha}(1 - \exp(-\alpha t))\exp\left(\gamma_1 \phi_{rf}\right) + 2a\sum_{n=1}^{\infty} B_n[\alpha \cos(n\omega t) + n\omega \sin(n\omega t)]\exp\left(\gamma_1 \phi_{rf}\right) + \exp\left(\gamma_1\left(\phi_{rf} - 1\right) - \alpha t\right), \quad (14)$$

with

$$a = \frac{j_i \exp\left(\phi_{fl}\right)}{C_1 + C_2}, \quad (15)$$

$$A = a[\exp(\phi_b) S_1 I_0(\gamma_2 \overline{\phi_{rf}}) + S_2 I_0(-\gamma_1 \overline{\phi_{rf}})], \quad (16)$$

$$B_n = \frac{S_2 I_n\left(-\gamma_1 \overline{\phi_{rf}}\right) + \exp(\phi_b) S_1 I_n\left(\gamma_2 \overline{\phi_{rf}}\right)}{\alpha^2 + n^2 \omega^2}. \quad (17)$$

Separating stationary, oscillatory, and transient terms, the expression of the analytical solution for ϕ becomes

$$\exp(\phi) = \frac{A}{\alpha}\exp\left(\gamma_1 \phi_{rf}\right) + 2a\sum_{n=1}^{\infty} B_n[\alpha \cos(n\omega t) + n\omega \sin(n\omega t)]\exp\left(\gamma_1 \phi_{rf}\right) + \exp(-\alpha t)\left[\exp\left(\gamma_1\left(\phi_{rf} - 1\right)\right) - \frac{A}{\alpha}\exp\left(\gamma_1 \phi_{rf}\right)\right]. \quad (18)$$

Still using the Modified Bessel functions to write $\exp(\gamma_1 \phi_{rf})$, stationary, oscillatory, and transient terms appearing in Eq. (10) are

$$S = \frac{\exp\left(\phi_{fl}\right)}{S_1 + S_2}\left\{\exp(\phi_b) S_1 I_0\left(\gamma_2 \overline{\phi_{rf}}\right) + S_2 I_0\left(-\gamma_1 \overline{\phi_{rf}}\right)\right\} I_0\left(\gamma_1 \overline{\phi_{rf}}\right), \quad (19)$$

$$T = \exp(-\alpha t)\left[\exp\left(\gamma_1\left(\phi_{rf} - 1\right)\right) - \frac{A}{\alpha}\exp\left(\gamma_1 \phi_{rf}\right)\right], \quad (20)$$

$$W = 2a\sum_{n=1}^{\infty} B_n[\alpha \cos(n\omega t) + n\omega \sin(n\omega t)]\exp(\gamma_1 \phi_{rf}). \quad (21)$$

III. EQUIVALENT MAGNETIZED PLASMA MODEL

The same model can be applied to a magnetized plasma. In this case, the asymmetry comes from the anisotropic medium and then from the magnetic topology. The surfaces to compare are the electrode surfaces perpendicular to the magnetic field and the perpendicular surface across which displacement currents occur (see Figure 3). The surface of the rf biased flux tube acts as a large capacitor.

If the main perpendicular current comes from the ion polarization drift[19] due to a time variation of the perpendicular electric field $E_\perp$, this current can be written as follows:

$$j_\perp = \frac{n_i m_i}{B^2}\frac{dE_\perp}{dt} \quad (22)$$

with n_i as the ion density, m_i as the ion mass, and B as the magnetic field strength. This current is mainly carried by ions because of their larger Larmor radius compared to electrons. These polarization currents can be very large around the ion cyclotron frequency, as it is the case close to ICRF antennas in tokamaks.[20] A dedicated model has been elaborated to study the impact of these currents onto the rectified potential along the flux tube[13] supposing a constant potential along the field line length $L_\parallel$. Using $L_\perp$ as the perpendicular scale for polarization currents,[15,22] the electric field can be linearized: $E_\perp = V/L_\perp$. The equivalent perpendicular capacitance can now be derived from the current $I = jS_\perp = C_\perp dV/dt$ as it is

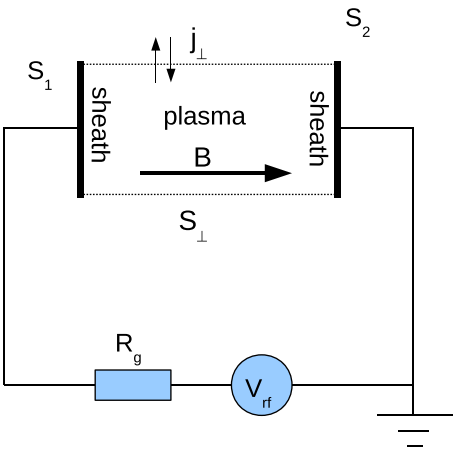

FIG. 3. Physical sketch of a magnetized flux tube exchanging rf currents.

done by Verplancke in his probe model,[23] using $S_\perp = L_\parallel L_\perp$ the perpendicular displacement current surface

$$C_\perp = \frac{n_i m_i L_\parallel}{B^2}. \tag{23}$$

Now considering the same perfect parallel conductor plasma, $V = V_1 = V_2$ and $S = S_1 = S_2$ for a constant magnetic field, the electrical model in Figure 4 is simplified, plasma resistance disappears and $C_\perp$ is in parallel with C_2. The equation to solve becomes

$$\begin{aligned} &j_i S\left(2 - \exp\left(-\phi + \phi_{fl}\right)\left[1 + \exp\left(\phi_{rf} + \phi_b\right)\right]\right) \\ &+ \frac{k_B T_e}{e}\left[C_1 \frac{d\left(\phi - \phi_{rf}\right)}{dt} + \left(C_2 + C_\perp\right)\frac{d\phi}{dt}\right] = 0. \end{aligned} \tag{24}$$

The solution is then exactly the same as in Section II, except that the former C_2 is replaced by C_h, a hybrid capacitance combining C_2 and $C_\perp$

$$C_h = C_2 + C_\perp. \tag{25}$$

This model can then be applied either to an asymmetric rf discharge or to a symmetric magnetized rf plasma on condition to know the perpendicular capacitance of the magnetized flux tube.

IV. ANALYTIC STUDY OF ASYMPTOTIC REGIMES FOR POTENTIALS AND CURRENTS

The analytic solution (10) is not straightforward in the physical meaning. Moreover, the main physical behaviour of

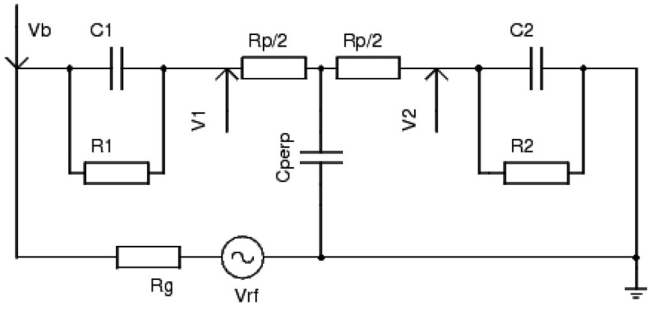

FIG. 4. Equivalent electric model of the magnetized plasma and sheaths.

the rectified potential and current can be described by asymptotic solutions of Eq. (10). This is what is done in this section, first presenting the no sheath capacitance limit case and next an infinite sheath capacitance.

A. No sheath capacitance

Here, the displacement currents in the sheath are neglected: C_1 and $C_2 \to 0$.

1. Rectified potential

Ignoring the transient term in Eq. (10), the solution for the potential in the plasma ϕ is

$$\phi = \phi_{fl} + \ln\left(\frac{S_2}{S_1 + S_2}\right) + \ln\left[1 + \frac{S_1}{S_2}\exp\left(\phi_{rf}\right)\right]. \tag{26}$$

One recovers the classical rf rectified potential[21] for a symmetric discharge $S_1 = S_2$ with $\overline{\phi_{rf}} > \phi_{fl}$

$$\phi = \phi_{fl} - \ln(2) + \ln[1 + \exp\left(\phi_{rf}\right)]. \tag{27}$$

The well known time averaged value for the rf potential is then $\langle\phi\rangle = \phi_{fl} + \frac{\phi_{rf}}{\pi}$.

2. Current

Introducing the previous potential solution in the current formula on the rf or the grounded electrode, it comes out

$$\langle I_1\rangle = -\langle I_2\rangle = j_i S_1 \left\langle \frac{1 - \exp\left(\phi_{rf}\right)}{1 + \frac{S_1}{S_2}\exp\left(\phi_{rf}\right)} \right\rangle. \tag{28}$$

This current is null for a symmetric discharge ($S_1 = S_2$).

If $S_1/S_2 \gg 1$, $\langle I_1\rangle$ saturates at $j_i S_2/2$ and for $S_1/S_2 \ll 1$, $\langle I_1\rangle$ saturates at $-j_i S_2/2$, while the electron saturation current is not reached, which means $S_2/S_1 < j_e/j_i$ in the case $S_1/S_2 \ll 1$.

B. Infinite sheath capacitance

In this particular case, $\alpha \to 0$ (see Eq. (11)).

1. Rectified potential

From Eq. (18), and still ignoring the transient term, the expression for ϕ can be reduced as follows:

$$\exp(\phi) = \frac{A}{\alpha}\exp\left(\gamma_1 \phi_{rf}\right), \tag{29}$$

which yields the following solution for the rectified potential in the plasma using the Bessel functions:

$$\begin{aligned} \phi &= \phi_{fl} + \gamma_1 \phi_{rf} \\ &+ \ln\left(\frac{\exp(\phi_b) S_1 I_0\left(\gamma_2 \overline{\phi_{rf}}\right) + S_2 I_0\left(-\gamma_1 \overline{\phi_{rf}}\right)}{S_1 + S_2}\right). \end{aligned} \tag{30}$$

One can see that the oscillatory terms disappear in the logarithm. The solution is purely sinusoidal because displacements currents are much higher than nonlinear

conduction currents. And the time averaged solution is of the order of the rf potential amplitude.

2. Current

In this high capacitive regime and for $S_1 \ll S_2$, the following lines demonstrate the current saturates at $I_{sat} = j_i S_2$ while $\overline{\phi_{rf}}$ is much higher than ϕ_{fl}

$$\begin{aligned}\langle I_2 \rangle &= -\langle I_1 \rangle \\ &= j_i S_2 \left(1 - \frac{\langle \exp(-\gamma_1 \phi_{rf}) \rangle}{\exp(\phi_b) S_1 I_0\left(\gamma_2 \overline{\phi_{rf}}\right) + S_2 I_0\left(-\gamma_1 \overline{\phi_{rf}}\right)}\right) \\ &= j_i S_2 \left(1 - \frac{I_0\left(-\gamma_1 \overline{\phi_{rf}}\right)}{\exp(\phi_b) S_1 I_0\left(\gamma_2 \overline{\phi_{rf}}\right) + S_2 I_0\left(-\gamma_1 \overline{\phi_{rf}}\right)}\right) \\ &= j_i S_2 \left(1 - \frac{1}{\exp(\phi_b) S_1 I_0\left(\overline{\phi_{rf}}\right) + S_2}\right). \end{aligned} \tag{31}$$

For $\overline{\phi_{rf}} > \phi_{fl}$, then $I_0(\overline{\phi_{rf}}) \gg 1$

$$I_2 = -I_1 \approx I_{sat}. \tag{32}$$

One finds exactly the same results than for a magnetic plasma flux tube with perpendicular currents[17] in which $C_\perp$ is high. With a magnetic field, as it is shown in Eq. (24), the main displacement currents come from perpendicular polarization currents proportional to the effective perpendicular surface around the flux tube.

C. Transition capacitance

This section is dedicated to find C_0 the transition capacitance under which the capacitance is considered as "low." The first approach consists in linearizing Eq. (1) for a small rf potential perturbation and the second one considers a saturated regime in which the current is equal to $I_{sat}/2$, which is the case for high capacitances and high rf potentials.

1. Linear regime

By linearizing Eq. (1), which means $\overline{\phi_{rf}} < \phi_{fl}$, the displacement current term is equivalent to the conduction term for $j_i = \omega k_B T_e C_1/(eS_1)$. In the same way, linearizing Eq. (7) leads to $j_i = \omega k_B T_e C_2/(eS_2)$. One deduces that the linear criterion to minimize the displacement current is as follows:

$$C_0^{lin} = \frac{j_i min(S_1, S_2)}{\omega} \frac{e}{k_B T_e}. \tag{33}$$

To be neglected, C_0^{lin} depends on the smaller electrode. The relevant capacitance to be compared to respect the criterion is the highest: $C = max(C_1, C_2)$. Finally, for $C/C_0^{lin} < 1$, the capacitance can be neglected and for $C/C_0^{lin} > 1$ the capacitance is considered as "high."

2. Saturated regime

For high rf potentials and highly asymmetric electrode surfaces, the condition changes: $j_i/2 \gg C\omega\tilde{\phi}/S_2$ with $\tilde{\phi}$ the amplitude of the fundamental harmonic of the noncapacitive solution according to Eq. (26) ($= \overline{\phi_{rf}}/2$).

Finally, it turns out

$$C_0^{sat} = \frac{j_i S_2}{\omega \overline{V_{rf}}}. \tag{34}$$

This criterion is much more appropriate to a strongly asymmetric discharge.

D. Typical asymmetric plasma discharge case

In most rf plasma discharges, the surface of the grounded wall S_2 is several times higher than S_1, the RF electrode surface. Consequently, $C_2 \gg C_1$ inducing $\gamma_1 \to 0$ and $\gamma_2 \to 1$. Moreover, capacitive currents can be neglected at low frequency, $\omega \ll \omega_{pe}$. For that particular set of parameters, the potential in the plasma is given by Eq. (26) and the current by Eq. (28).

This analytical result does not take into account the plasma resistivity and more important the RF generator typical resistance which often equals 50 Ω. To consider this resistance, the set of equations of the first part has to be solved numerically and yields some results which can be far from the "ideal" analytical case.

The 3 relevant parameters conditioning the DC current asymmetry are the surface ratio of electrode and wall S_1/S_2, the RF voltage with respect to floating potential V_{rf}/V_{fl}, and the normalized capacitance ratio C/C_0. The next step consists in validating the code with these 3 parametric sweeps to approach the asymptotic analytical solutions given by Eqs. (28) and (32).

V. NUMERICAL RESULTS

The solving of the system composed of Eqs. (1), (7), and (8) yields the solutions for the 3 unknowns V_1, V_2, and V_b from which the currents I_{gnd} ($= I_2$) and I_{rf} ($= I_1$) flowing through both sheaths on the wall and RF sides, respectively, can be derived as a function of time.

A. Surface ratio analysis

First, we want to check the formula (28) for parameters close to most RF plasma discharges. The internal impedance of the RF amplifier is set to 5 Ω and the frequency to 1.356 MHz to check the model. The classical value is 50 Ω for impedance and 13.56 MHz for frequency but this needs to increase the rf voltage to reach the good conditions to match formula (28). Sheath capacitances are input according to formula (3) and (4) depending on the surface ratio S_1/S_2 swept from 0.01 to 100. The plasma resistivity is calculated from a plasma density of 10^{15} m^{-3}, the typical cross section for a cold Argon gas at a pressure of 2×10^{-2} mbar, and an electron temperature of 2 eV. And the plasma resistance is deduced from the resistivity for a 1 m long plasma with an average cross section of $(S_1 + S_2)/2$. The typical plasma resistance is here 4.4 Ω.

We are interested in the time average value of the current in each sheath over one rf period, so each dataset is averaged to plot the DC current normalized to the saturation

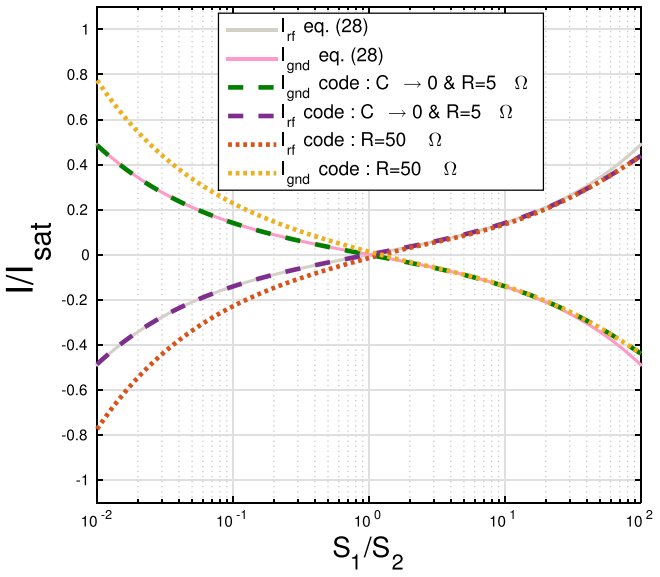

FIG. 5. Comparison of the numerical current solution and the analytical current considering $V_{rf} \gg V_{fl}$ as a function of the cathode to anode surface ratio S_1/S_2 for R = 5 Ω.

current $j_i.S_2$ as a function of the surfaces ratio S_1/S_2 of the rf electrode and the grounded wall.

First of all, the current conservation shown in Figure 5 is clearly verified because the total current collected on the RF electrode is exactly the opposite of the current collected by the grounded wall. Second, the DC current equals 0 for a symmetric discharge ($S_1 = S_2$). This DC current is negative on the RF electrode for $S_1/S_2 < 1$ (most of rf discharges). And the same DC current is positive for $S_1/S_2 > 1$. The analytical formula (28) matches very well the solution of the code for a small capacitance and a small resistance, while for the typical capacitance in Eqs. (3) and (4), the current can overpass half the saturation current.

B. RF voltage analysis

Here, the discharge parameters are exactly the same as before except the rf potential is now swept from 1 V to 1000 V and the electrode surface ratio is fixed at 0.01. For RF potential lower than the floating potential (9.35 V), no net dc current is driven. If sheaths are not capacitive, then the dc current saturates at half the ion saturation current $I_{sat}/2$. Figure 6 confirms the validity of the code for low capacitance (C → 0) and low resistance (R = 5 Ω) because the corresponding curve matches the analytic equation (28). For typical parameters of a plasma discharge, the saturation limit for the current can overpass $I_{sat}/2$, while for a much higher capacitance, the current behavior approaches the analytical solution (31) corresponding to an infinite capacitance limit. In this case and for a low generator resistance (R = 0.1 Ω), the current saturation limit is I_{sat}.

The typical case for our plasma discharge is plotted in Figure 6(c) for which the generator impedance of 5 and 50 Ω and the typical capacitance C_1 and C_2 for each sheath are input in the code according to their definition in Eqs. (3) and (4). The capacitance values depends on the rf potential applied because the sheath thickness is proportional to $V_{rf}^{3/4}$. Thus,

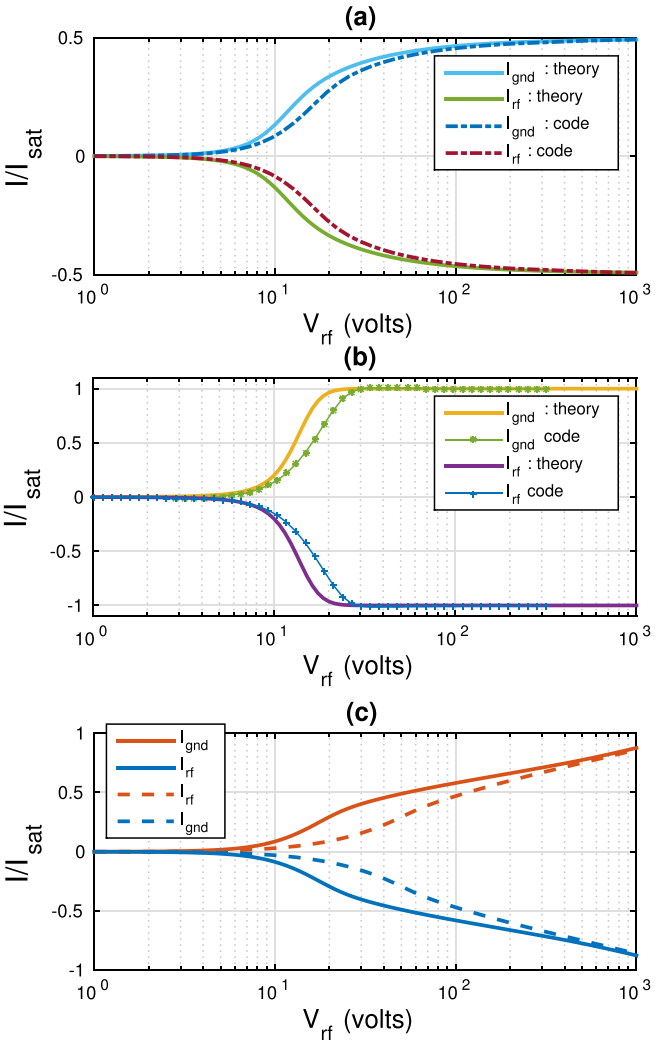

FIG. 6. Normalized current as a function of the rf potential on the rf electrode. In figure (a) $C \to 0$: the solid line curves are plotted from the theoretical model (Eq. (28)) and the dashed curve from the code for $R_g = 5\,\Omega$. In figure (b) $C = 100C_0$: the solid line curves are plotted from the theoretical model (Eq. (31)) and the dashed curve from the code for $R_g = 0.1\,\Omega$. In figure (c) $C = max(C_1, C_2) \approx C_0$: the solid and dashed curves are plotted from the code for $R_g = 5\,\Omega$ and $R_g = 50\,\Omega$, respectively, and the typical value of C.

according to simulation parameters given at the beginning of Section V A, the ratio $max(C_1, C_2)/C_0$, C_0 being defined in Eq. (34), varies from 0.48 to 2.7 with respect to the rf potential variations from 1 V to 1000 V. One can see that the current saturation is not reached but this saturation tends to I_{sat}. The effect of the generator resistance is to shift the current characteristic to the high potential side or simply to decrease the current flowing through the circuit. The finite capacitance of order C_0 constrains the current between the low and high capacitance cases. Finally, for high rf potential values (over 200 V here), the 5 and 50 Ω curves join each other because the relative generator impedance becomes small compared to the global impedance including the sheath and the saturation is not reached even for a 1000 V rf potential.

C. Capacitance analysis

We have seen that Eq. (28) expresses the dc current solution for a low sheath capacitance, and for high sheath

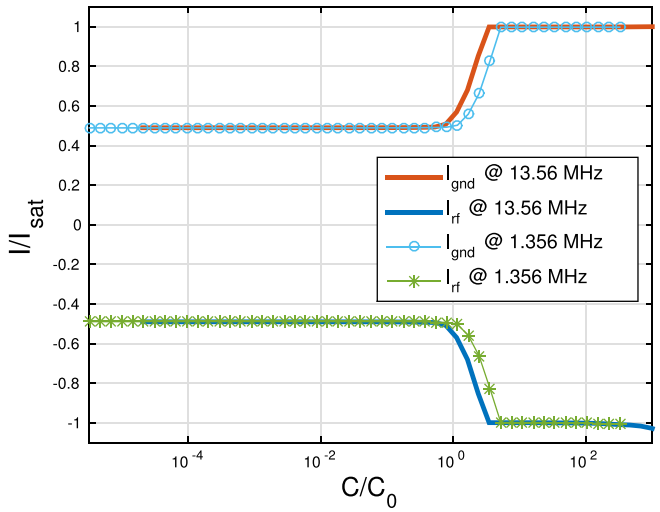

FIG. 7. Normalized current as a function of the normalized sheath capacitance C/C_0 with $C = max(C_1, C_2)$. In that case $C_0 = C_0^{sat}$ defined in Eq. (34).

capacitance the solutions obeys Eq. (31). The transition between these 2 regimes can be seen in Figure 7 for C/C_0 close to 1 with the transition capacitance $C_0 = C_0^{sat}$ as defined in Eq. (34). These results are summarized in Table I. One can check as well the validity of the transition capacitance C_0 at which the current saturation is suddenly doubled for two values of the rf frequency (1.356 and 13.56 MHz) because the transition capacitance is inversely proportional to the rf frequency. Here, simulations are performed with $R = 0.1\ \Omega$. For $R = 5\,\Omega$ and $R = 50\,\Omega$, the current curve remains exactly the same and are not plotted here. In that range of parameters, the resistance of the generator is much lower than the sheath resistance so that it does not disturb the saturation transition which mainly depends on the sheath capacitance. Regimes with high generator resistance or low sheath resistance are not described in this paper but can be exactly calculated by the code.

VI. CONCLUSION

The asymmetric electric double probe model presented here is directly connected to RF generator via the generator resistance instead of the usual blocking capacitor used in most plasma discharges. Consequently, this model allows DC current to flow through the circuit. The analytical formula deduced from the model describe how dc current are influenced by sheath capacitance, electrode surface ratio, plasma and generator resistances, and the applied rf potential.

The main results of this model are (1) dc currents saturate at $+I_{sat}/2$ or $-I_{sat}/2$ while $|S_1/S_2| \gg 1$, $\overline{\phi_{rf}} \gg \phi_{fl}$, and for a low sheath capacitance ($C < C_0$). The linear and saturated transition capacitances C_0^{lin} and C_0^{sat} are defined as well. (2) In the same conditions but for a high sheath capacitance ($C > C_0$), currents saturate at $+I_{sat}$ or $-I_{sat}$. (3) The current direction is controlled by the surface ratio, if S_1/S_2 is smaller than 1 the current collected on S_1 (the rf electrode surface) is negative, and in the other case the current is positive. (4) An analytic solution of the rf averaged rectified potential and current in a perfect conductor plasma is also given as a function of the electrode surface ratio, the rf potential, and sheath capacitance. (5) The same analytical solution can be used as well for a symmetric rf magnetized plasma considering perpendicular polarization currents that can be evaluated through an effective perpendicular capacitance. (6) A simplified analytical solution is given for the dc current on each side of the discharge for 2 asymptotic regimes (low capacitance and infinite capacitance). (7) And the full circuit model is solved numerically and yields the exact solution of the time dependent rf potential and current at both sheath edges and on the rf antenna. The numerical model takes into account the generator resistance, constant plasma conductivity, sheath capacitances, rf potential applied on the antenna, and all other plasma parameters. The code is validated by asymptotic current formulas.

TABLE I. Asymptotic dc current on rf electrode as a function of sheath capacitance and rf potential for $S_1/S_2 \ll 1$.

I_{rf}	$C < C_0$	$C > C_0$
$V_{rf} \le V_{fl}$	0	0
$V_{rf} \gg V_{fl}$	$-\frac{I_{sat}}{2}$	$-I_{sat}$

These results could help to better understand probe measurements in rf environment and without rf compensation. In addition, this model is useful in tokamaks in which different parts of the structure can be biased (e.g., antenna structure) relative to the grounded wall, inducing dc current between these points and modifying the average potential along the connected field lines. In other plasma devices, this model could be used to generate and control the dc current on a rf biased surface and could be applied to a magnetized plasma as well. One of the weakness of this model is the assumption concerning the flat geometry. To exactly take into account of the real electrode geometry and plasma shape, 3D models are necessary.

Now one have to validate experimentally the crude assumptions made in this circuit model, by measuring the potential at the entrance of the rf and grounded wall sheaths and the current flowing through the antenna. Finally, the plasma is supposed only resistive while in typical discharges one should take into account the plasma inductance and capacitance. This property could be added in future works.

ACKNOWLEDGMENTS

The author acknowledges the French National Research Agency through Contract No. ANR-12-JS09-0013-01 SPICE RF for its financial support.

[1]P. Chabert and N. Braithwaite, *Physics of Radio-Frequency Plasmas* (Cambridge University Press, 2011).
[2]M. A. Lieberman and A. J. Lichtenberg, *Principles of Plasma Discharges and Materials Processing*, 2nd ed. (John Wiley and Sons, Inc., Publication, 2005).
[3]M. A. Lieberman, J. Appl. Phys. **65**, 4186 (1989).
[4]M. A. Lieberman and S. E. Savas, J. Vac. Sci. Technol. **A8**, 1632 (1990).
[5]A. Metze, D. W. Ernie, and H. J. Oskam, J. Appl. Phys. **60**, 3081 (1986).
[6]F. F. Chen, Plasma Sources Sci. Technol. **15**, 773 (2006).
[7]P. A. Miller and M. E. Riley, J. Appl. Phys. **82**, 3689 (1997).

[8]M. A. Sobolewski, Phys. Rev. E **56**(1), 1001–1011 (1997).
[9]M. A. Sobolewski, Phys. Rev. E **62**(6), 8540–8553 (2000).
[10]M. Klick, Phys. Rev. E **47**(1), 591–603 (1993).
[11]R. Van Nieuwenhove and G. Van Oost, Plasma Phys. Controlled Fusion **34**(4), 525–532 (1992).
[12]E. Faudot, S. Devaux, J. Moritz, S. Heuraux, P. Molina Cabrera, and F. Brochard, Rev. Sci. Instrum. **86**, 063502 (2015).
[13]E. Faudot, S. Heuraux, and L. Colas, Phys. Plasmas **13**, 042512 (2006).
[14]E. Faudot, L. Colas, S. Heuraux, and J. P. Gunn, Phys. Plasmas **17**, 042503 (2010).
[15]D. A. D'Ippolito *et al.*, Nucl. Fusion **42**, 1357–1365 (2002).
[16]K. Gunther and A. Carlson, Contrib. Plasma Phys. **34**(2/3), 484–489 (1994).
[17]E. Faudot, S. Heuraux, M. Kubic, J. Gunnand, and L. Colas, Phys. Plasmas **20**, 043514 (2013).
[18]M. A. Lieberman, IEEE Trans. Plasma Sci. **17**(2), 338 (1989).
[19]A. V. Nedospasov and D. A. Uzdensky, Contrib. Plasma Phys. **34**, 478 (1994).
[20]J.-M. Noterdaeme and G. Van Oost, Plasma Phys. Controlled Fusion **35**, 1481–1511 (1993).
[21]A. Godyak and A. A. Kuzovnikov, Fiz. Plazmy **1975**, 496–503.
[22]A. Ngadjeu, E. Faudot, L. Colas, S. Heuraux, J. Gunn, and M. Kubi, J. Nucl. Mater. **415**, S1009–S1012 (2011).
[23]P. H. Verplancke, R. Chodura, J.-M. Noterdaeme, and M. Weinlich, Contrib. Plasma Phys. **36**(S), 145–150 (1996).